remote sensing

MDPI

Article

Energy-Barycenter Based Waveform Centroid Algorithm for Pulse Lidar Ranging System

Baoling Qi [1,2], Lijun Wang [3], Dongbin Guo [1] and Chunhui Wang [1,2,*]

[1] National Key Laboratory of Tunable Laser Technology, Harbin Institute of Technology, Harbin 150001, China
[2] Geling Institute of AI and Robotics, Shenzhen 518063, China
[3] School of Optoelectronic Engineering, Chongqing University of Posts and Telecommunications, Chongqing 400065, China
* Correspondence: wang2352@hit.edu.cn

Abstract: This paper proposes an energy-barycenter-based waveform centroid algorithm (EWCA) for a high-precision Lidar ranging system. Firstly, the emission and echo pulse models of the pulse Lidar ranging system are established. Secondly, based on analyzing the merits and demerits of the conventional waveform centroid algorithm (CWCA) and intensity-weighted waveform centroid discrimination algorithm (IWCD). Moreover, combined with the characteristics of the energy moment distribution, the adaptive strategy is used to select the point with the higher signal as the calculation time series, and we proposed the EWCA to calculate the timing moment. Finally, we compared EWCA with CWCA and IWCD through simulation and actual experiments. The experimental simulation results show EWCA has higher accuracy and robustness than the comparison algorithm with different SNR. EWCA can achieve an average error of 0.1235 ns, a standard deviation of 0.0848 ns, and variance of 0.0072 ns at an SNR of 5 dB. At the same time, the Lidar ranging system is established to compare these methods further, and the ranging error of the proposed method can be within 20 mm when the measured distance is 40 m. This method has higher timing accuracy and application range, which has the potential to handle further ranging tasks.

Keywords: energy-barycenter; waveform centroid algorithm; Lidar; rang accuracy

Citation: Qi, B.; Wang, L.; Guo, D.; Wang, C. Energy-Barycenter Based Waveform Centroid Algorithm for Pulse Lidar Ranging System. *Remote Sens.* **2022**, *14*, 3938. https://doi.org/10.3390/rs14163938

Academic Editor: Pinliang Dong

Received: 6 July 2022
Accepted: 10 August 2022
Published: 13 August 2022

1. Introduction

The pulsed Lidar ranging system is based on the principle of pulse time-of-flight (ToF) ranging. Pulse ToF ranging takes advantage of the characteristics of the concise duration of a laser pulse, relatively concentrated energy in time, and large instantaneous power. Under the safe condition of specific average laser power, it can achieve long-distance measurement. It has a wide range of applications in many fields, such as autonomous driving [1], three-dimensional shape measurement [2], three-dimensional object scanning [3], and intelligent mobile robot technology [4], which puts forward higher requirements for the accuracy of laser ranging systems.

A pulsed laser is used as the light source to emit a pulse with a narrow pulse width to the target, and the distance is measured by calculating the time difference between the echo pulse and the transmitted pulse. For a Lidar system, most previous works focused on improving the accuracy of time measurement. The main ranging methods can be divided into time identification methods based on the time-to-digital converter (TDC) and waveform centroid determination. When the environment and the target are more complex, the amplitude of the echo pulse changes greatly, and the TDC technology that only relies on the threshold to achieve time measurement will no longer be suitable, leading to a large drift error [5–8]. The full waveform ranging method is the most effective method to solve this problem, mainly including the waveform centroid and Gaussian fitting methods. The Gaussian fitting algorithm sets the initial Gaussian parameters according to the echo waveform. It uses the least square method to update the iterative Gaussian waveform

parameters to obtain the optimal solution. The fitting iteration takes a long time and is complicated to implement in hardware [9–12]. The waveform centroid algorithm uses the time-weighted average method to extract the echo time. Due to its simple algorithm and fast execution speed, it is widely used and studied [13–16]. A time window is set to select the effective calculation point, and then the centroid point is calculated by the waveform centroid algorithm. The proposed algorithm can eliminate certain noise through filtering, but its calculation point is selected by using a fixed window width, resulting in poor applicability. Its analysis shows that the laser echo signal is a Gaussian-like waveform with energy concentrated in the middle [14]. Li et al. [17] proposed an IWCD method to calculate the intensity weight of each point, and then measure the centroid. Although the intensity value change is considered, it does not select the calculation points, and this calculation method is too scattered. Therefore, it is necessary to study the selection of critical points of the centroid algorithm and make full use of the practical information of the full-waveform echo signal by combining it with the actual waveform.

In this paper, aiming at the requirements of the pulse Lidar ranging system for higher accuracy, we propose the energy barycenter-based waveform centroid algorithm. The signal's energy is conserved in the time domain and the frequency domain. In the time domain, the signal's energy can be obtained by the sum of the squares of the discrete points. The main lobe of the waveform, which has the most useful information, is selected by the adaptive strategy. Then the waveform centroid algorithm based on energy-barycenter is proposed to calculate the time. The effectiveness and feasibility of the algorithm are verified through simulation and actual experiments on the Lidar ranging system.

2. Lidar System Models

2.1. Transmitted Pulse Model in the Lidar System

The pulse Lidar detection system adopts the ToF method for ranging. ToF is used to measure the time interval between the transmitted laser pulse and the echo laser pulse. The trailer of the transmitted pulse can be ignored, and its time domain envelope approximates to Gaussian:

$$S_{tr}(t) = \sum_{m=1}^{\infty} A \exp\left(-4\ln 2\left(\frac{t - mT_R}{\tau_{3dB}}\right)^2\right), \tag{1}$$

where $S_{tr}(t)$ is the model of transmitting pulse signal at time t; A is the amplitude of transmitted laser pulse; τ_{3dB} is the full pulse width corresponding to 3 dB bandwidth; m is the number of pulses; T_R is the pulse repetition period.

2.2. Echo Pulse Model in the Lidar System

The detection of echo pulse signal can be described by Gaussian function and corresponding characteristic parameters [18]

$$S_{ec}(t) = \sum_{m=1}^{\infty} \alpha \frac{q_e}{T_0} \exp\left(-4\ln 2\left(\frac{t - mT_R - 2R/c}{\tau_{3dB}}\right)^2\right) + N_n, \tag{2}$$

where $S_{ec}(t)$ is the model of the echo pulse signal at time t; α is the echo energy attenuation coefficient; q_e is the energy of the transmitted pulse signal; T_0 is the pulse width of laser; R is the distance between the target and the laser source of the Lidar system; c is the speed of light in vacuum; N_n is the random additive noise. In the actual measurement, there are some non-ideal factors in the signal, such as atmospheric turbulence and attenuation, background noise, and detection noise.

The time interval t_τ between the transmitted pulse and the echo pulse equals twice the distance between the target and the laser emitter divided by the speed of light. Therefore, the distance between Lidar and the target can be calculated by:

$$R = \frac{1}{2} c t_\tau, \tag{3}$$

In this paper, the detection target of the Lidar system is mainly unmanned vehicles, the detection environment is roads, and the main detection range is from several meters to several hundred meters. Therefore, the atmospheric environment is relatively stable, and the influence of atmospheric turbulence and attenuation on echo pulse is relatively slight. The background noise and other target interactions may affect the shape and amplitude of the pulse waveform. We set the ratio between the mean peak power received on the detector and the root mean square of the photoelectronic chain without signal as the SNR.

3. The Waveform Centroid Algorithm Analysis

3.1. Conventional Waveform Centroid Algorithm (CWCA)

The conventional waveform centroid algorithm records the entire waveform amplitude and corresponding time information through the analog-to-digital converter (ADC). Analyze the shape and position of the entire waveform, and then calculate the geometric center of the waveform. By discretely sampling the waveform, the waveform centroid can be calculated as follows:

$$t_z = \frac{\sum_{i=1}^{n} iy_i}{\sum_{i}^{n} y_n}, \quad u_z = \frac{\sum_{i=1}^{n} iy_i}{n}, \tag{4}$$

where t_z is the centroid moment of the echo pulse; u_z is the centroid amplitude of the laser pulse; i is the corresponding sampling point number; n is the total number of the sampling points, and y_i is the amplitude of echo sample points of the echo pulse.

The result of Equation (4) depends on the waveform of the entire echo, which is affected by the data length and the relative amplitude of the sampling points. The whole waveform will inevitably be distorted due to environmental interference, including dark current and detector noise. The changes are due to less available information but more excellent noise. Therefore, the weighted average of the entire waveform data may easily lead to a drift in the calculations centroid.

3.2. Intensity-Weighted Waveform Centroid Discrimination Algorithm (IWCD)

This method is an improved algorithm based on the conventional waveform centroid algorithm. The IWCD calculates the intensity weighting factor W_i by sampling points of the waveform:

$$W_i = \frac{1}{\sum_{j=1, j\neq i}^{n} R_{ij}}, \tag{5}$$

where $R_{ij} = P_j/P_i, i = 1, 2, \ldots, n, j = 1, 2, 3 \ldots n; j \neq i$; the sampling point of the echo pulse waveform is expressed as $P_i(y_i, t_i)$.

Furthermore, the waveform centroid of the IWCD can be calculated as follows:

$$t_{iwc} = \frac{\sum_{i}^{n} t_i W_i}{\sum_{i}^{n} W_i}, \quad u_{iwc} = \frac{\sum_{i}^{n} t_i W_i}{\sum_{i}^{n} t_i}, \tag{6}$$

where t_{iwc} is the centroid moment of the echo pulse; u_{iwc} is the centroid amplitude of the laser pulse; t_i is the corresponding moment of each pulse.

From the time of the IWCD echo calculation moment, the average wave of ups and downs intensity factor is recorded, which can smooth the waveform distortion to a certain extent. On the one hand, the overall intensity of each point has to be calculated resulting in a lack of information and noise to distinguish the weights. On the other hand, it depends on the sampling rate, which significantly limits its applicability.

3.3. Energy-Barycenter Based Waveform Centroid Algorithm (EWCA)

The signal's energy is conserved in the time and frequency domains. In the time domain, the signal's energy can be obtained by summing all discrete points squared. Through repeated experiments, we found that in the actual pulse Lidar system, the emission and echo waveform are Gauss-like waveforms, so they have the characteristics of Gaussian distribution. Its energy in the peak range of the main lobe can represent the energy of the entire waveform, that is, it represents most of the effective information. In order to solve the shortcomings of the above algorithms and combine the characteristics of energy distribution in the signal, the EWCA algorithm is proposed. The implementation of the proposed algorithm has been illustrated in Figure 1. It mainly includes the following stages:

1. Select the sampling points. Calculate the slope of each point and record the maximum and minimum slopes of the sampling points at the corresponding time. The sampling sequence from the time corresponding to the maximum slope, to the time corresponding to the minimum slope is selected;
2. Determine whether the main lobe peak is included. Judge whether the peak point is included in the sampling sequence. If included, proceed to step 4. Otherwise, proceed to step 3;
3. Select a new sampling sequence. When the slope sequence does not meet the condition of including the peak value, the point between the full width at half maximum (FWHM) is selected as the sampling point sequence;
4. The energy-barycenter based waveform centroid algorithm is used to calculate the arrival time of the echo. Calculate the arrival time of the echo through EWCA, and then the time interval between transmitted pulses is calculated to obtain the measured distance.

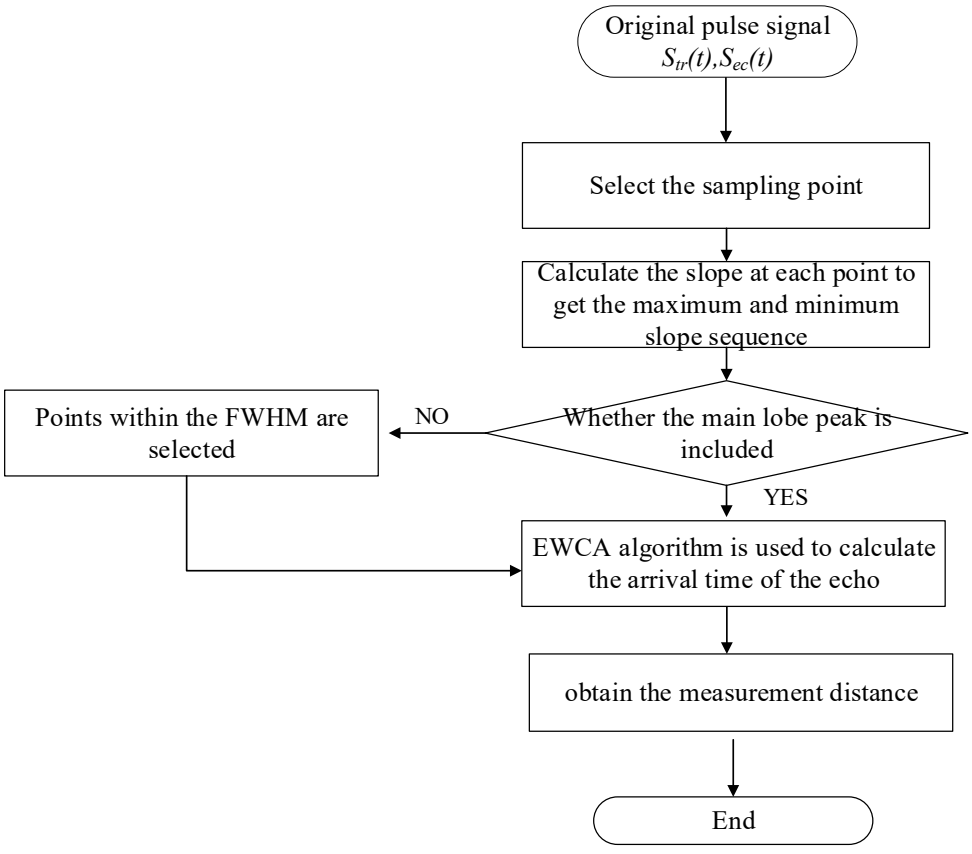

Figure 1. The flow chart of the proposed EWCA method.

Combined with the characteristics of the energy-barycenter centroid distribution, a torque is generated after rotating around the origin of the energy coordinate at a time t_i, which is defined as an energy moment, and the value of the energy moment is:

$$I_i = E_i t_i, \tag{7}$$

where t_i is the corresponding moment of each sampling point of each pulse; E_i is the energy value at the time t_i, and then the total energy moment of the entire sequence of sampling points is calculated as:

$$I_{sum} = \sum_{i=1}^{k} E_i^2 t_i, \tag{8}$$

where $\sum_{i=1}^{k} E_i^2$ is the total energy. We assume that all the energy in all moments falls on the time coordinate t_i, and set $E_i = y_i$ in the pulse waveform.

When the moment of energy reaches equilibrium, suppose that the sequence points we obtain through the point selection strategy are (t_i, y_i) where $i = 1, 2, \cdots, k$, which can calculate the time domain energy. The echo time calculated by EWCA is:

$$t_{ECWA} = \frac{\sum_{i}^{k} t_i E_i^2}{\sum_{i}^{k} E_i^2} = \frac{\sum_{i}^{k} t_i |y_i|^2}{\sum_{i}^{k} |y_i|^2}, \quad y_{ECWA} = \frac{\sum_{i}^{k} t_i |y_i|^2}{\sum_{i}^{k} t_i}, \tag{9}$$

where t_{EWCA} is the centroid moment of the echo pulse; y_{EWCA} is the centroid amplitude of the laser pulse; E_i is the energy at the corresponding moment, and t_i and y_i are the corresponding moments of the laser pulse and the amplitude of the sampling point of the echo pulse, respectively. Record the pseudocode of the EWCA algorithm in Algorithm 1.

Algorithm 1. Pseudocode for EWCA

The reference and the echo Lidar signals S_{tr}, S_{ec} were input
The slope sequences S_{tr_slope} and S_{ec_slope} of Lidar signal were calculated, respectively
Input the reference signal S_{tr} and the echo signal S_{ec}, respectively, and calculate their slope sequences $S_{tr\_slope}, S_{ec\_slope}$ respectively
Calculate the beginning and end of the slope sequence
$S_{tr\_slope\_start}$ = the maximum value of S_{tr_slope}
$S_{tr\_slope\_end}$ = the minimum value of S_{tr_slope}
$S_{ec\_slope\_start}$ = the maximum value of S_{ec_slope}
$S_{ec\_slope\_end}$ = the minimum value of S_{ec_slope}
If (the minimum to maximum slope interval contains the maximum values of S_{tr}, S_{ec})
    for each point in the slope sequence
        The centroid time and centroid amplitude of EWCA reference and echo signals were calculated by Equation (9)
    end for
else
    for each point in the FWHM sequence
        The centroid time and centroid amplitude of EWCA reference and echo signals were calculated by Equation (9)
    end for
end if
return $P\_sr(X\_sr\_EWCA, Y\_sr\_EWCA)$,$P\_ec(X\_ec\_EWCA, Y\_ec\_EWCA)$

The points between the maximum and minimum slopes are selected as the main lobe sequence sampling points, which have the largest part of the effective signal energy of the laser pulse and can well represent the pulse signal. Our algorithm does not depend on the overall smooth waveform and increases the proportion of valid signals to suppress

interference clutter noise. The moment is calculated when the signal moment of energy reaches equilibrium in the waveform centroid, and the selection of points does not depend on the fixed window function. It has a certain degree of self-adaptation, which can meet the application of engineering.

4. Simulation Analysis

The parameters of the Lidar system in the simulation are set as follows: the sampling frequency is 5 Gsa/s, the transmitted pulse width with 3 dB is 4 ns, the pulse repetition frequency is 200 kHz, and the distance to the target is 50 m.

In Figure 2a, the transmitted and the echo pulse signals are shown. The pulse signal after the finite impulse response (FIR) digital filter is shown in Figure 2b. Adding the FIR can eliminate the high-order frequency and the direct current component. It is more helpful for further research and analysis.

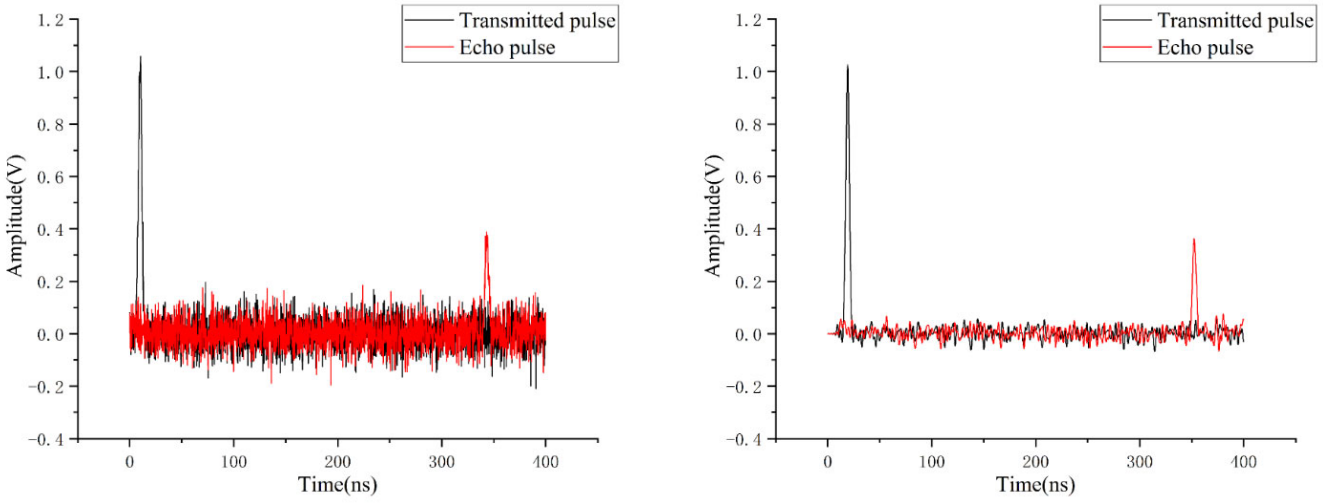

Figure 2. (**a**) Transmitted and echo pulse signal; (**b**) Transmitted and echo pulse signal after FIR.

Based on the same waveform, we repeated the experiments to eliminate the randomness of the results caused by random Gaussian white noise. Within the scope of the SNR for 5–15 dB, with 1 dB as the step value, for each 10,000 times simulation experiments under SNR. The average absolute error, standard deviation, and variance of the three algorithms under different SNRs are shown in Table 1, respectively.

Table 1. The timing performance of the three algorithms under different SNR.

SNR (dB)	Average Time Error (ns)			Standard Deviation (ns)			Variance (ns)		
	CWCA	IWCD	EWCA	CWCA	IWCD	EWCA	CWCA	IWCD	EWCA
5	45.6039	0.1663	0.1235	17.6129	0.1617	0.0848	62.2137	0.0262	0.0072
6	35.2123	0.1678	0.0965	15.1467	0.1351	0.0704	57.5210	0.0183	0.0050
7	29.4283	0.1593	0.0781	11.0965	0.1429	0.0576	53.1320	0.0204	0.0033
8	24.1494	0.1592	0.0663	8.4397	0.1552	0.0498	45.2288	0.0241	0.0025
9	18.9067	0.1560	0.0594	7.0873	0.1041	0.0448	40.2299	0.0108	0.0020
10	15.2086	0.1566	0.0569	5.9159	0.1369	0.0425	34.9983	0.0187	0.0018
11	17.2132	0.1552	0.0538	5.2481	0.1093	0.0418	27.5424	0.0119	0.0018
12	10.9086	0.1555	0.0576	4.5167	0.1094	0.0436	20.4010	0.0120	0.0019
13	10.8383	0.1566	0.0552	4.0168	0.1519	0.0444	16.1348	0.0231	0.0020
14	8.9395	0.1560	0.0483	3.5012	0.1241	0.0446	12.2585	0.0154	0.0020
15	6.7230	0.1555	0.0455	2.8880	0.1322	0.0477	8.3407	0.0150	0.0023

As shown in Table 1, the CWCA algorithm significantly differs in error and stability compared with the IWCD and EWCA. Therefore, the error comparison of the latter two algorithms is mainly made, and the error distribution diagram of the IWCD and EWCA algorithms is made, as shown in Figure 3.

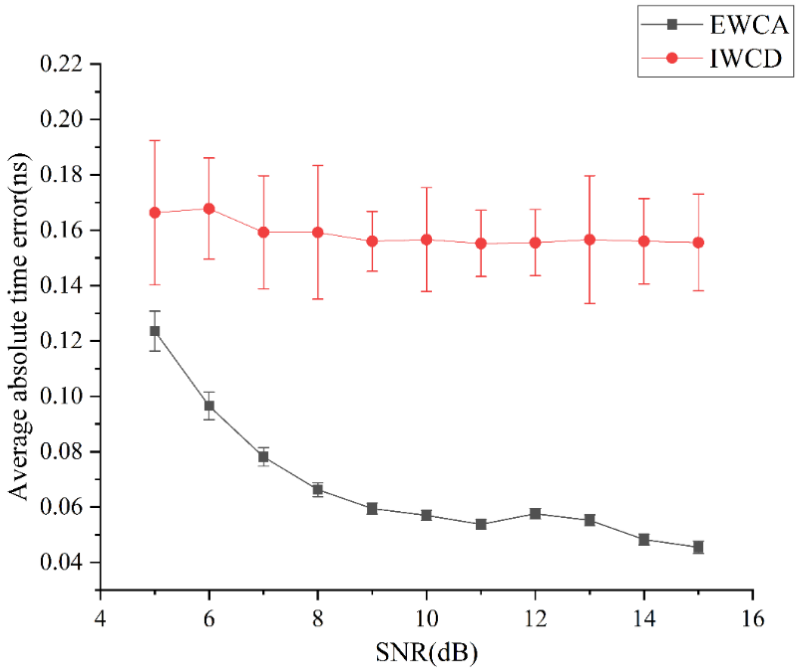

Figure 3. The error distribution diagram of the IWCD and EWCA under different SNR.

According to Figure 3, it can be found that the average absolute time error of the proposed algorithm is smaller than the IWCD under the simulation repeated experiment, and the effect is more obvious with the improvement of SNR. It shows that the EWCA has a better timing accuracy, that is, it has higher ranging accuracy under simulation experiments. Furthermore, the standard deviation is smaller, which means that the sensitivity of the proposed algorithm has better robustness for noise than the IWCD.

5. Experiments and Evaluation

5.1. Experimental System Description

The actual environment and the Lidar system are different from the simulation. On the one hand, the simulation is idealized. That is, the noise type cannot represent the actual scene. On the other hand, the waveform emitted by the laser source is not a standard Gaussian waveform but a Gaussian-like waveform with a steep front and a slow back. Therefore, we built a Lidar system to verify the proposed method's performance in the actual scene. The principle of the pulse Lidar ranging system is shown in Figure 4 in this paper. The laser emits laser pulses through the beam splitter with a beam splitter ratio of 95/5. The beam split ratio of 95 is used as the measuring light path to reach the target through the MEMS micro-mirror. The detector receives the waveform reflected by the target. The beam splitter ratio of 5 is used as the local oscillator light and reaches the detector as a reference clock signal. The signal processing part calculates the time difference between the transmitted and the echo pulses, and the built-up pulse Lidar ranging system is shown in Figure 5. The relevant parameters of the system are listed in Table 2.

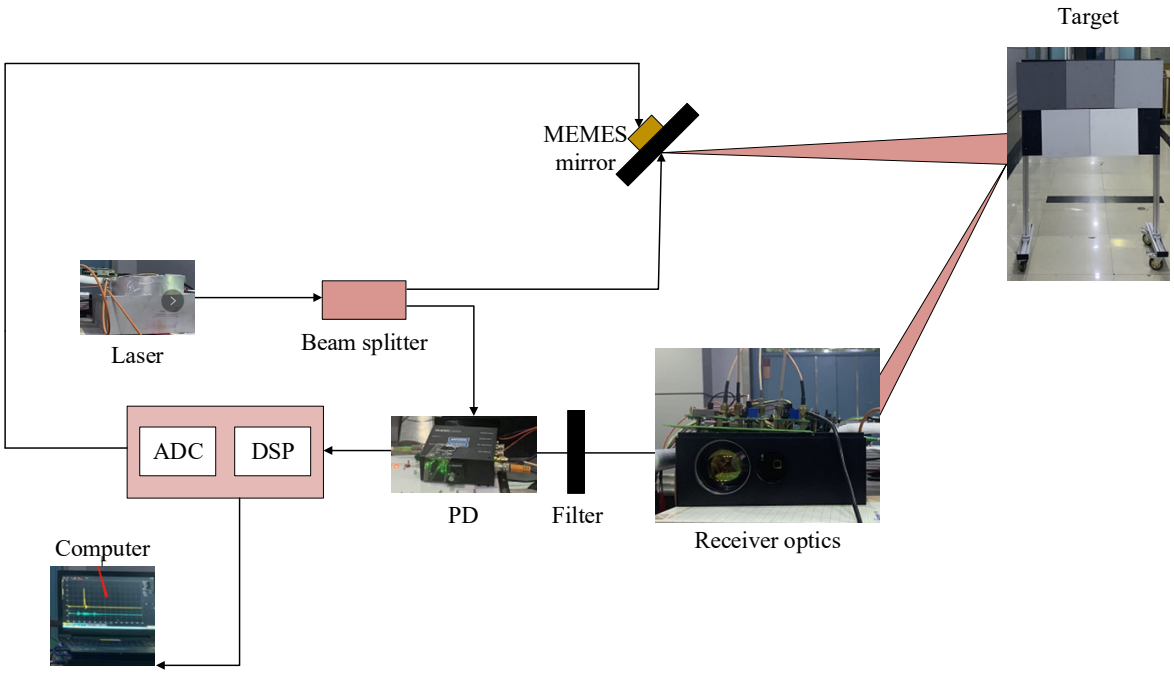

Figure 4. Principle diagram of the pulse Lidar ranging system. ADC is analog to digital converter, DSP is digital signal processing.

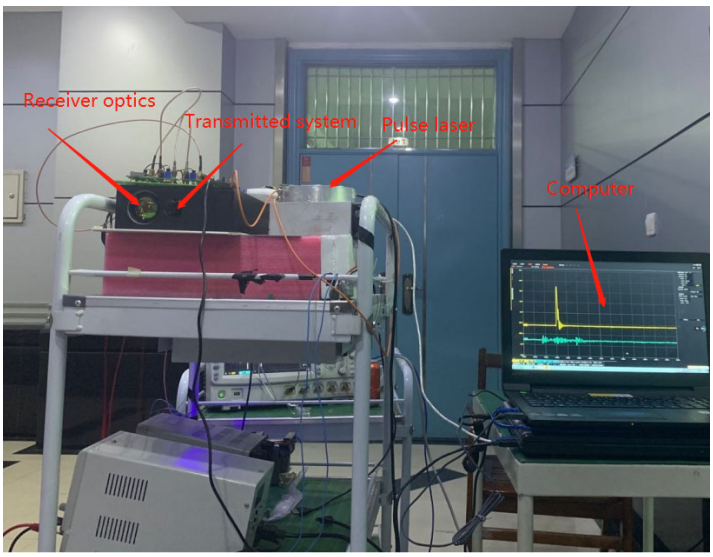

Figure 5. Experimental equipment diagram of the pulse Lidar ranging system.

Table 2. Specifications of the Lidar system.

Parameter	Value
Laser wavelength	1064 nm
Pulse width	4 ns
Model of APD	PDB430C
APD response frequency band	250 MHz
Size of APD photosensitive surface	3 mm
Receiving system optical aperture	50 mm
ADC sampling rate	5 GSa/s
ADC bandwidth	1 GHz

5.2. Experimental Results and Analysis

The BOSCH GLM500 laser (BOSCH, Gerlingen, Germany) rangefinder is used to calibrate the standard distance, and its ranging accuracy is ±1.5 mm, which is used to calibrate the target position at the distance of 25 m, 30 m, 35 m, and 40 m. Through repeating 50 experiments for each position, the data sampled by the oscilloscope are recorded, and the relevant data are processed offline on the computer. The calculated pulse centroid is shown in Figure 6, where the actual sampling of the avalanche APD is negative. In order to show an intuitive comparison, we perform a positive-negative conversion on the sampling pulse. The recorded results of the experiment are shown in Table 3.

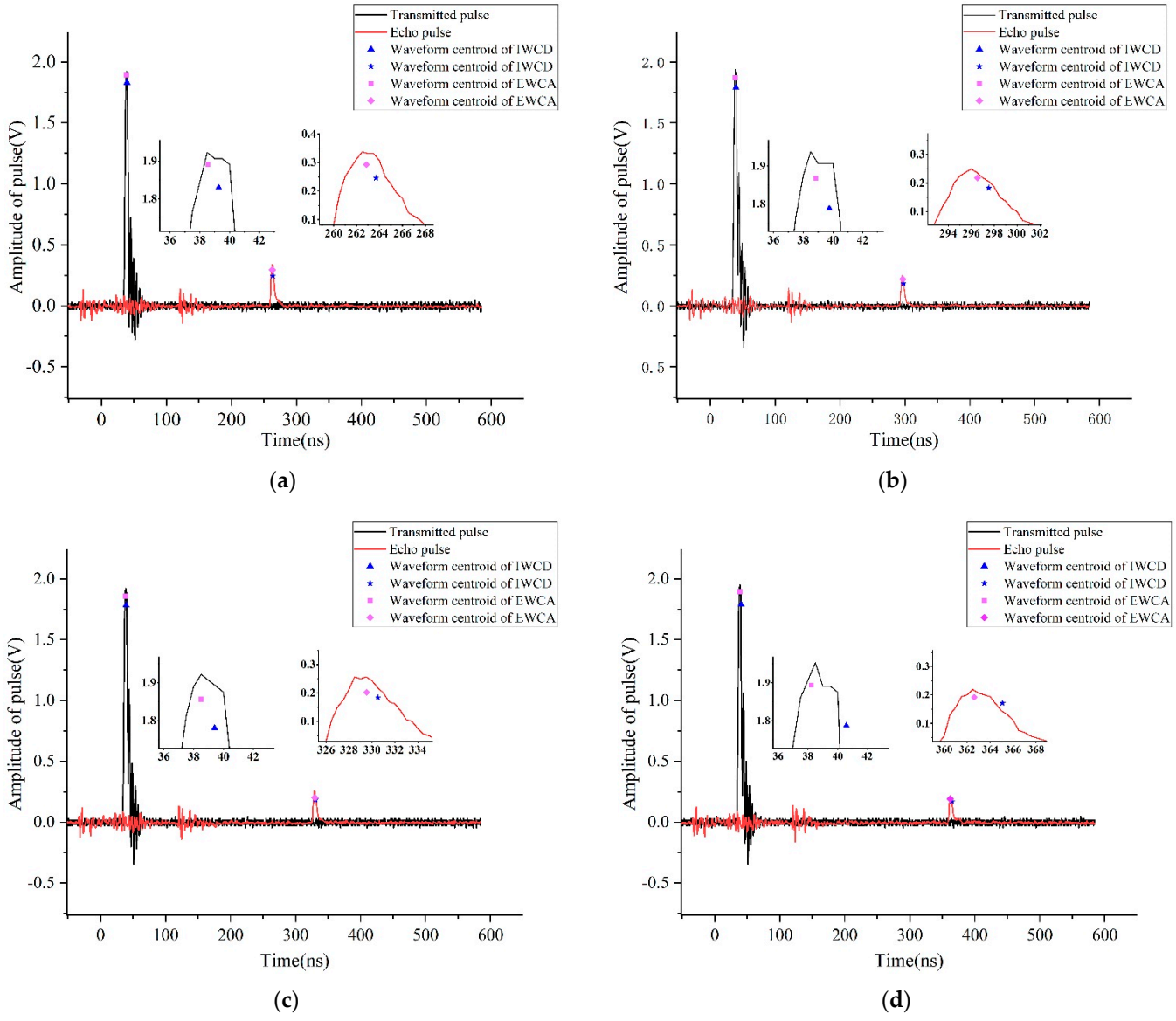

Figure 6. The calculated centroid points of the transmitted and the echo pulses: (**a**) measure the target distance at 25 m (**b**) measure the target distance at 30 m (**c**) measure the target distance at 35 m (**d**) measure the target distance at 40 m.

Table 3. Ranging results of the algorithms.

Distance (m)	Average Time Error (ns)		Average Distance Error (mm)	
	IWCD	EWCA	IWCD	EWCA
25	0.167	0.076	25	11
30	0.182	0.088	27	13
35	0.196	0.102	29	15
40	0.220	0.114	33	17

As shown in Table 3, the average time error of the EWCA is smaller than the IWCD, and the distance measurement accuracy is higher, consistent with the previous simulation conclusions. In Table 3, we find that as the distance increases, the time measurement error also increases, but it remains within the range of 0.1 ns. From the results of measuring the distance error, it can be seen that under the same distance, the relative IWCD error of the EWCA is reduced by about half. The signal-to-noise ratio decreases mainly due to the system's dark current and the Lidar system's equipment delay. Further improvement of hardware equipment and high-speed AD can further improve the accuracy of the Lidar ranging system.

The sampling pulses and centroid calculation are shown in Figure 6, and our method can identify the center of gravity of the pulse very well. In this paper, in order to further verify the effectiveness of the proposed algorithm, on the premise of not changing the Lidar setup and optical path, the target is set at a distance of 20 m from the Lidar, and the standard reflectance plates with different reflectance are used to replace the detection targets. By setting different standard reflectivity plates of 20–75%, the echo laser pulses with different SNRs are simulated, as shown in Figure 7. Because the experimental environment is indoors and the external atmospheric environment is relatively stable, background noise interference (such as sunlight and other light sources) can be almost ignored. Here, we take the average value of the echo signal shown in Figure 7 as the base signal, superimpose white Gaussian noise with the same SNR on it, and then use different time measurement algorithms to calculate 1000 times. By calculating the mean absolute time error (MATE) of distance measurement under different algorithms, we draw the results with boxes, which can visually display the maximum and lowest error interval and the overall error distribution, as shown in Figure 8.

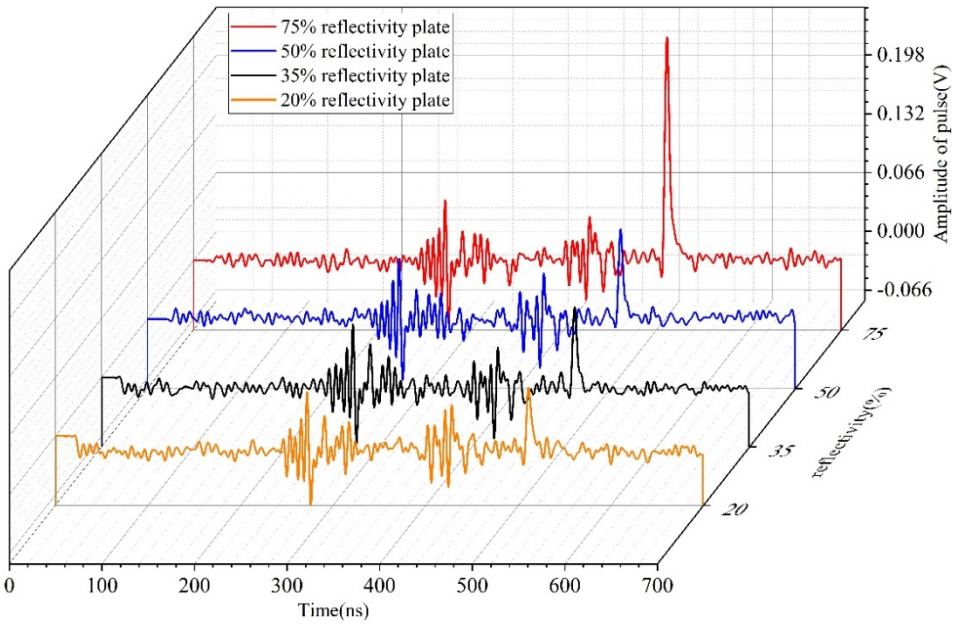

Figure 7. Echo pulse of different reflectivity targets at 20 m.

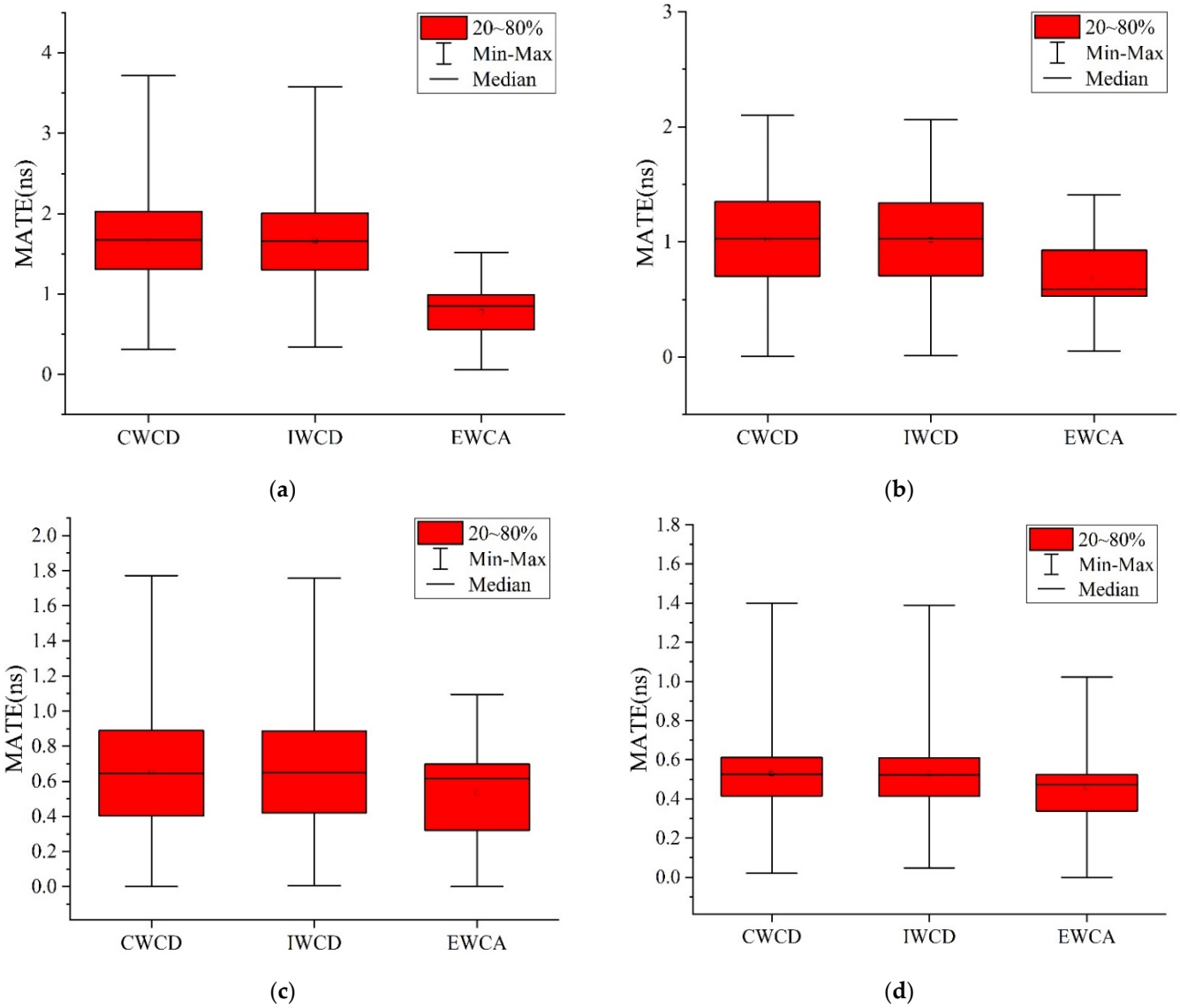

Figure 8. Mean absolute time error distribution diagram of different reflectance boards at 20 m: (**a**) the reflectance of the measurement target is 20% (**b**) the reflectance of the measurement target is 35% (**c**) the reflectance of the measurement target is 50% (**d**) the reflectance of the measurement target is 75%.

The above figure shows that the EWCA algorithm has advantages under 35% and 20% target reflectance plates. In a complex environment, the overall ranging error is relatively concentrated. Compared with the comparison algorithm, the EWCA has better accuracy and stability. Furthermore, in order to visually display and compare the ranging performance of the algorithm, we set the maximum acceptable error as 1 ns, which means that the ranging error in this range represents the DSR (detection success rate). The proportion of successful experiments is taken as the DSR, and the experimental results are recorded in Table 4.

As seen from the table, the proposed algorithm can accurately detect target distance under different echo SNRs, that is, targets with different reflective characteristics. According to the detection success rate, we can see that our algorithm has better environmental adaptability and can achieve an 81.4% detection success rate even with a 20% low reflectance target, which is significantly improved compared with the comparison algorithm. However, under the high SNR target of 75% reflectance, there is little difference between the calculated

points, resulting in little difference in the ranging accuracy among the three algorithms. Therefore, the effectiveness and applicability of the proposed algorithm are demonstrated from the perspective of accuracy and stability through several different experiments.

Table 4. The mean absolute time error and detection success rate under different reflectivity plates.

Reflectivity (%)	MATE (ns)			DSR (%)		
	CWCD	IWCD	EWCA	CWCD	IWCD	EWCA
20	1.6775	1.6603	0.7788	5.4	5.4	81.4
35	1.0199	1.0165	0.6826	46.3	46.7	94.7
50	0.6538	0.6607	0.5356	87.3	88.4	99.4
75	0.5065	0.5043	0.4445	100	100	100

6. Conclusions

In this paper, we proposed the energy barycenter-based waveform centroid algorithm, which meets the increased requirements for high precision pulse Lidar ranging systems under different SNR environments. Based on the analysis of conventional centroid and intensity-weighted waveform centroid discrimination algorithms, and combined with the idea of energy distribution, the time solution formula of the improved algorithm is obtained and corresponding simulations and experiments are carried out, respectively. Compared with the IWCD in the simulation results, the EWCA has a smaller ranging error and standard deviation under different signal-to-noise ratios. Considering the difference between the actual environment and the simulation, we built a set of Lidar systems to conduct experiments under different distances and different reflectance target plates. The experiments on an actual Lidar ranging system show that the ranging accuracy at different distances is better than the IWCD algorithm. The ranging error can be within 20 mm when the measured distance is 40 m. Several experiments were carried out by superimposing simulated noise based on 20 M different reflectance plates as the primary signal. Compared with the comparison algorithm, the proposed method can achieve a more than 80% detection success rate under 20% and 35% low reflectance targets. Therefore, the effectiveness and feasibility of the algorithm proposed in this paper are fully proved. The EWCA waveform centroid algorithm improves the computational complexity to a certain extent because the waveform centroid algorithm essentially depends on the selection of calculation points. Hence, the computational effort in this aspect is essential. Moreover, with the emergence of high-speed ADC and high-performance FPGA, the system delay can be further reduced, and it is more hopeful of achieving better results. The proposed algorithm has the potential to be applied to Lidar systems.

Author Contributions: B.Q. conducted the simulations and experiments and completed the manuscript; L.W. carefully improved the presentation of the manuscript; D.G. participated in data curation and plotting; C.W. modified the manuscript. All authors have read and agreed to the published version of the manuscript.

Funding: This work was supported by the National Key Scientific Instrument and Equipment Development Projects of China (Grant No. 62027823) and Shenzhen Fundamental Research Program (Grant No. JCYJ2020109150808037).

Data Availability Statement: Not applicable.

Acknowledgments: The authors would like to thank T.C. for supplying guidance in circuit design.

Conflicts of Interest: The authors declare no conflict of interest.

References

1. Hongji, H.; Yuchun, Y.; Guan, G.; Hikmet, S. Deep Reinforcement Learning for UAV Navigation Through Massive MIMO Technique. *IEEE Trans. Veh. Technol.* **2020**, *69*, 1117–1121.
2. Mohammadikaji, M.; Bergamann, S.; Irgenfried, S.; Beyerer, J.; Dachsbacher, C.; Worn, H. A framework for uncertainty propagation in 3d shape measurement using laser triangulation. In Proceedings of the 2016 IEEE International Instrumentation and Measurement Technology Conference Proceedings, Taipei, Taiwan, 23–26 May 2016; IEEE: Piscataway, NJ, USA, 2016.
3. Gallay, M.; Hochmuth, Z.; Kanuk, J.; Hofierka, J. Geomorphometric analysis of cave ceiling channels mapped with 3-D terrestrial laser scanning. *Hydrol. Earth Syst. Sci.* **2016**, *20*, 1827–1849. [CrossRef]
4. Krivic, S.; Piater, J. Pushing corridors for delivering unknown objects with a mobile robot. *Auton. Robot.* **2019**, *43*, 1435–1452. [CrossRef]
5. Kurtti, S.; Jansson, J.P.; Kostamovaara, J. A CMOS Receiver—TDC Chip Set for Accurate Pulsed TOF Laser Ranging. *IEEE Trans. Instrum. Meas.* **2020**, *69*, 2208–2217. [CrossRef]
6. Chao, Z.; Lindner, S.; Antolovic, I.M.; Wolf, M.; Charbon, E. A CMOS SPAD Imager with Collision Detection and 128 Dynamically Reallocating TDCs for Single-Photon Counting and 3D Time-of-Flight Imaging. *Sensors* **2018**, *18*, 11.
7. Kurtti, S.; Nissinen, J.; Kostamovaara, J. A wide dynamic range CMOS laser radar receiver with a time-domain walk error compensation scheme. *IEEE Trans. Circuit. Syst. I-Regul. Pap.* **2017**, *64*, 550–561. [CrossRef]
8. Jie, C.; Qun, H.; Yang, C.; Yuxin, P.; Kaiyu, Z.; Jiaxing, M.; Peng, W. Differential time domain method improves performance of pulsed laser ranging and three-dimensional imaging. *Appl. Optics.* **2016**, *55*, 360–367.
9. Xiaolu, L.; Bingwei, Y.; Xinhao, X.; Duan, L.; Lijun, X. Influence of waveform characteristics on LiDAR ranging accuracy and precision. *Sensors* **2018**, *18*, 1156. [CrossRef] [PubMed]
10. Shiyu, Y.; Guohui, Y.; Qingyan, L.; Bin, Z.; Yu, W.; Yu, Z.; Chunhui, W. Distance-Intensity Image Strategy for Pulsed LiDAR Based on the Double-Scale Intensity-Weighted Centroid Algorithm. *Remote Sens.* **2021**, *13*, 432. [CrossRef]
11. Wu, Q.; Qiang, S.; Wang, Y. Continuous wavelet transform and iterative decrement algorithm for the Lidar full-waveform echo decomposition. *Appl. Opt.* **2019**, *58*, 9360.
12. Milutin, M.; Sebastian, S.; Johan, H.; Camillo, R.; Eva, L.; Markus, H.; Norbert, P.; Hakan, O. Influence of footprint size and geolocation error on the precision of forest biomass estimates from space-borne waveform LiDAR. *Remote Sens. Environ.* **2017**, *200*, 74–88.
13. Salas, E.A.L. Waveform LiDAR concepts and applications for potential vegetation phenology monitoring and modeling: A comprehensive review. *Geo-Spat. Inf. Sci.* **2020**, *24*, 179–200. [CrossRef]
14. Shiyu, Y.; Guohui, Y.; Qingyan, L.; Chunhui, W. Waveform centroid discrimination of pulsed Lidar by combining EMD and intensity weighted method under low SNR conditions. *Infrared Phys. Technol.* **2020**, *109*, 103385.
15. Muss, J.D.; Aguilar-Amuchastegui, N.; Mladenoff, D.J.; Henebry, G.M. Analysis of waveform lidar data using shape-based metrics. *IEEE Geosci. Remote Sens. Lett.* **2012**, *10*, 106–110. [CrossRef]
16. Fieber, K.D.; Davenport, I.J.; Ferryman, J.M.; Gurney, R.J.; Walker, J.P.; Hacker, J.M. Analysis of full-waveform LiDAR pulse properties for vegetation discrimination and characterisation. *ISPRS-J. Photogramm. Remote Sens.* **2013**, *82*, 63–82. [CrossRef]
17. Yunxi, L.; Tianxiang, C.; Qingyan, L.; Bin, Z.; Yuru, B.; Chunhui, W. Waveform centroid discrimination of return pulse weighting method in LIDAR system. *Optik* **2019**, *180*, 840–846.
18. Abdallah, H.; Baghdadi, N.; Bailly, J.S.; Pastol, Y.; Fabre, F. Wa-LiD: A new LiDAR simulator for waters. *IEEE Geosci. Remote Sens. Lett.* **2012**, *9*, 744–748. [CrossRef]